ISSN NO. 2320-5407

Journal homepage: http://www.journalijar.com

INTERNATIONAL JOURNAL OF ADVANCED RESEARCH

RESEARCH ARTICLE

Automatic deformity estimation and path tracing methodology for thoracic CT image sequences from inhale to exhale position.

***Ali Imam Abidi, and S. K. Singh**
Department of Computer Science & Engineering, IIT (BHU), Varanasi, India.

Manuscript Info

Manuscript History:

Received: 17 January 2016
Final Accepted: February 2016
Published Online: March 2016

Key words:
Deformable thoracic image sequence, SURF, Automatic control point selection, Deformity estimation, Path tracing.

******Corresponding Author***

Ali Imam Abidi.

Abstract

Often clinical studies on image based respiratory systems either suffer road blocks or yield inconsistent results due to artifacts from a variety of subjects' erratic breathing patterns. This leads to loss of resources and time to ultimately get inconclusive and potentially wrong results. The proposed work can be seen as an automatic way of computing average thoracic deformation for a set of diverse subjects. In an image sequence, corresponding control point pairs or landmarks can be used to define the internal deformations with respect to time, point of view or modality. Defining enough number of control points in a thoracic image temporal sequence to describe the deformations happening in it is a tedious task. This inspired the use of automatic definition of control points in the proposed work. The paper proposes an automatic registration process for tracing deformity paths of the thoracic region between full inhale and exhale positions based on Hessian-matrix based feature detector and Haar wavelets based descriptor along with Optical Flow Motion (OFM) estimation technique. The proposed work presents a unique and innovative arrangement of methods to compute the average deformation of the thoracic region from all anatomical positions. The credibility and performance of the above proposed method is demonstrated by its exemplary experimental results.

Introduction:-

Accounting for organ motion in image based lung cancer radiation treatment is considered as an important challenge in medical imaging [9]. Lung deformations have been constant focus of studies for the verification of medical imaging equipments and for medical training purposes for a long period of time and still, physiologically speaking, very little is understood about the respiratory movement [25]. The movement of the lung is passive; a result of the movement of other parts of the body, such as the diaphragm and the thoracic cage, and it is not possible to observe the lung directly, as it would collapse if the thoracic cage is opened. The clinical relevance of this research is diverse. Respiratory motion is related to the function of the lung and therefore a diagnostic value in itself [8]. Furthermore, breathing induced organ motion potentially leads to image artifacts and to position uncertainty in image guided procedures. Particularly in radiotherapy planning of thoracic and abdominal tumors, the respiratory motion causes important uncertainties and is a significant source of error [11]. Therefore, there has been a large and continuing growth in studies and applications of 4D CT images for motion measurement, radiotherapy treatment planning, as well as functional investigations [21]. "A non-invasive method to describe lung deformations was proposed using NURBS surfaces based on imaging data from CT scans of actual patients" [25, 29]. Zordan et al [34] created an anatomical inspired, physically based model of human torso for the visual simulation of respiration. It has been shown that breathing motion is not a robust and 100% reproducible process [18, 30] and now there is a widespread common consent that it would be useful to use prior knowledge of respiratory organ motion and its "variability to improve radiotherapy planning and treatment delivery" [6].

The framework that has been acquired in this article is that the constituents of a thoracic image sequence with starting frame as the full inhale and ending frame as the full exhale are compared to find a set of common feature points, only distinction in them being different coordinate values (may be) and that they exist in different temporal frames. These common feature points are collectively called as the corresponding feature set. This feature set then serves as input to an OFM estimation algorithm as control point cloud corresponding to the thoracic image sequence. The estimation algorithm then traces the deformation in the thoracic image sequence right through initial to final frame.

The role of image registration techniques is increasing in these applications. Image registration enables the estimation of the breathing-induced motion and the description of the temporal change in position and shape of the structures of interest by establishing the correspondence between images acquired at different phases of the breathing cycle. A variety of image registration approaches have been used for respiratory motion estimation in recent years [22]. Image Registration is the alignment/overlaying of two or more images so that the best superimposition can be achieved. These images can be of the same subject at different points in time, from different viewpoints or by different sensors. This way the contents from all the images in question can be integrated to provide richer information. It helps in understanding and thus reducing the differences occurred due to variable imaging conditions. Most common applications of Image Registration include remote sensing (integrating information for GIS), combining data obtained from a variety of imaging modalities (combining a CT and an MRI view of the same patient) to get more information about the disease at once, cartography, image restoration etc. An image registration method targets to find the optimal transformation that aligns the images in the best way possible. If the underlying transformation model allows local deformations, i.e. nonlinear fields' u(x), then it is called Deformable Image Registration (DIR) [17].

Image registration has been categorized into two kinds based on the type of image it is being applied for. The two kinds of images are Rigid Images and Deformable Images. Rigid images are those of structures with rigid morphological properties e.g. bones, buildings, geographical structures etc. Deformable images are those of structures shape and size of which can be modeled after tangible physically deformable models [24]. Rigid image registration although is an important aspect of registration it is not the topic of discussion in this article. Since the discussion is about Medical Image Registration and almost all anatomical parts or organs of the human body are deformable structures, the concentration here is on DIR [19].

One of the three basic categories of physical models [16] conceptually utilized in this article is the Diffusion models. Thirion, inspired by Maxwell's Demons [28], proposed to perform image matching as a diffusion process, his work in turn inspired most of the work done in image registration using diffusion models [27]. Peyrat et al. used multi-channel Demons to register time-series of cardiac images by enforcing trajectory constraints [20]. Each time instance was considered as a different channel while the estimated transformation between successive channels was considered as constraint. Yeo et al. [33] derived Demons forces from the squared difference between each element of the Log-Euclidean transformed tensors while taking into account the reorientation introduced by the transformation.

A safer and more accurate evaluation of the respiratory movement will help in the selection of the appropriate medicine, the determination of the effectiveness of a treatment, to reduce the number of cases of clinical trial, observe the progress of rehabilitation treatments, among other possible applications. The present work uses a novel and never-tried-before automatic approach for deformity estimation in a temporal sequence of thoracic CT images.

Material and Methods:-

The dataset used comprised of a total (3×6)×10 i.e. 180 thoracic CT images across 10 subjects. There were 6 frames from a temporal thoracic image sequence each for every Anatomical Plane (AP) i.e. Axial (supine), Coronal and Sagittal for all the 10 subjects acquired simultaneously with a gap of 0.1 second starting from time t= 0 and ending at 0.6 seconds. All images were identified as $I_N^{AP}(x, y, t)$ where $\{N, t \in \mathfrak{R}^+ \mid 1 \le N \le 10; 0.1 \le t \le 0.6\}$ (x, y) coordinates in the Cartesian plane, t being the timestamp at which the particular frame/image was recorded, N would be the number assigned to the test subject and *AP* signifies the three anatomical planes of view i.e. Axial (a), Coronal (c) and Sagittal (s). So, the sixth subject's Coronal CT image acquired at t=0.3 sec would be identified as

$I_6^c(x, y, 0.3)$. Samples of images used from all viewpoints and all subjects from timestamps 0.1 to 0.6 seconds are summarized in Table 1.

Table 1: Working database through all anatomical planes from t=0.1 to 0.6 sec

ANATOMICAL PLANES $(0.1 \le t \le 0.6)$			
	Axial	**Coronal**	**Sagittal**
1	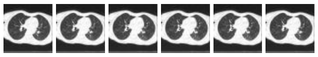	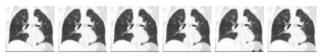	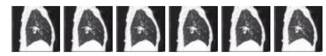
2	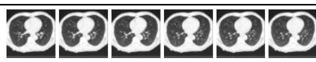		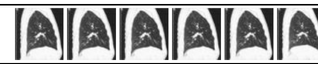
3	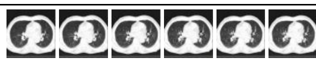	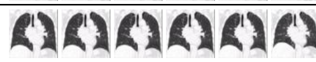	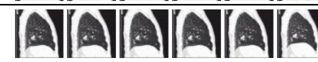
4	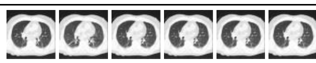	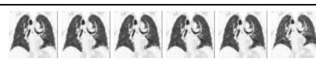	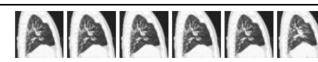
5	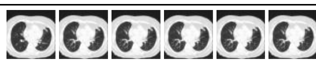	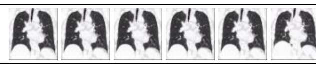	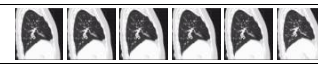
6	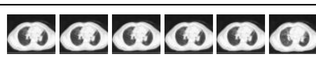		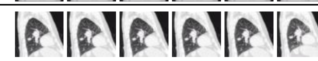
7	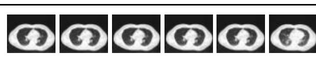		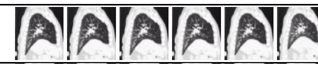
8	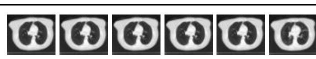	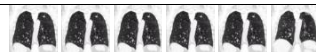	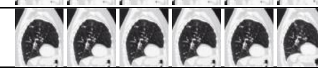
9	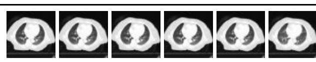	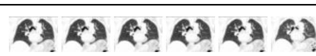	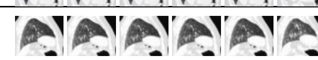
10		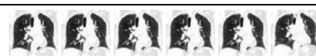	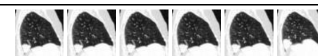

The procedure acquired is as such that a temporal thoracic image sequence from time t=0.1 to 0.6 sec is taken such that first frame of the sequence is the full inhale frame and the last frame is full exhale frame. This paper uses the Speeded up Robust Feature detector (SURF) [4, 3] to obtain a feature set comprising of common feature points throughout the image sequence. It detects and describes the feature set irrespective of any scaling and /or rotation in the corresponding images. SURF provides better approximations in comparison to previously proposed schemes with respect to repeatability, distinctiveness, and robustness, yet can be computed and compared much faster than any other state of the art feature detector. These feature sets are then fed into the OFM estimation algorithm to identify the deformation path throughout the temporal sequence, be it peripheral or local. This complete process is shown in figure 1.

Optical flow has been successfully applied to motion estimation of points/point clouds and other point set surface definitions over a temporal sequence [26]. It performs better than its contemporaries while tracing deformations that are realistic and guides the user in manipulation of real-world objects. It also allows the user to specify the deformations using either sets of points or line segments, the later useful for controlling curves and profiles present in the image. For each of these techniques, it provides simple closed-form solutions that yield fast deformations, which can be performed in real-time. The proposed methodology aims to track and estimate the deformations by tracking the transition of the interest points through the sequence from full inhale to full exhale frame.

Figure 1: (a) the proposed framework structure, (b) the working of SURF

A novel scale- and rotation-invariant detector and descriptor, has been coined as Speeded-Up Robust Features (SURF) by Herbert Bay et.al in 2006 [4] and 2008 [3]. It provides better approximations in comparison to previously proposed schemes with respect to repeatability, distinctiveness, and robustness, yet can be computed and compared much faster.

Focus is on scale and in-plane rotation-invariant detection and descriptions. These seem to offer a good compromise between feature complexity and robustness to commonly occurring photometric deformations in thoracic images. Skewing, anisotropic scaling, and perspective effects are assumed to be second order effects, that are covered to some degree by the overall robustness of the descriptor. For guaranteed invariance to any scale changes the input thoracic images are analyzed at different scales. The detected interest points are provided with a rotation and scale-invariant descriptor.

The detector is based on Hessian matrix based on its good performance in accuracy [3]. Blob-like structures are detected at locations with maximum determinant. In comparison to the Hessian-Laplace detector [15] Hessian determinant is used for scale selection [14].

Given a point a = (x, y) in an image I_N^{AP} ,the Hessian matrix $\hat{H}$(a, σ) at scale σ is defined as follows:

$$\hat{H}(a,\sigma) = \begin{bmatrix} L_{xx}(a,\sigma) & L_{xy}(a,\sigma) \\ L_{xy}(a,\sigma) & L_{yy}(a,\sigma) \end{bmatrix} \qquad (1)$$

where $L_{xx}(a,\sigma)$ is the convolution of the Gaussian second derivative $\partial g(\sigma) / \partial a^2$ with the image I_N^{AP} at point *a*, similarly for $L_{xy}(a,\sigma) \,\&\, L_{yy}(a,\sigma)$.

Though, Gaussians are optimal for scale-space analysis [13], they have to be made discrete and cropped in practice. This results in loss in repeatability of the detector for thoracic CT image rotations around odd multiples of π/4.

The SURF method consists of multiple stages to obtain relevant feature points from a sequence of thoracic images. The single SURF stages are:

1. An integral image is constructed for each frame of the input thoracic image sequence, it allows for fast computation of box type convolution filters [31]. This enables very few memory accesses and hence results in drastic improvement in computational time [7], which is especially crucial when we are dealing with a sequence of images. An integral image $I_{N\,\Sigma}^{AP}(a)$ at a location *a*= (x, y)^T represents the sum of all pixels in the input image I_N^{AP} within a rectangular region formed by the origin and ***a***.

$$I_{N\,\Sigma}^{AP}(a) = \sum_{i=0}^{i\le x} \sum_{j=0}^{j\le y} I_N^{AP}(i, j) \qquad (2)$$

2. Candidate feature points are searched by the creation of a Hessian scale-space pyramid (SURF detector). Approximation of the Hessian as a combination of box filters allows fast filtering. High contrast feature points are selected.
3. Feature vector is calculated (SURF descriptor) based on its characteristic direction to provide rotation invariance. Feature vector is normalized for immunity to changes in lighting conditions.
4. Matching of descriptor vectors between the thoracic image sequence frames using distance measures such as Mahalonobis distance and Euclidean distances etc.

Optical flow is the pattern of apparent motion of objects, surfaces, and edges in a visual scene caused by the relative motion between an observer (an eye or a camera) and the scene [32]. In recent times, the term optical flow has been co-opted by computer vision experts to incorporate related techniques from image processing and control of navigation, such as motion detection, object segmentation, time-to-contact information, focus of expansion calculations, luminance and motion compensated encoding and stereo disparity measurement [5]. Sequences of ordered thoracic images allow the estimation of motion as either instantaneous image velocities or discrete image displacements [1]. Barron et.al provided a performance analysis of a number of optical flow techniques. It emphasizes the accuracy and density of measurements [2].

Suppose we have a continuous thoracic image frame $I_N^{AP}(x, y, t)$; $f(x, y, t)$ refers to the gray-level of (x, y) at time t. It represents a dynamic thoracic image as a function of position and time. Few assumptions also work in hindsight:

- The detected feature point moves but does not actually change intensity.
- Feature point at location (x, y) in frame *i* is the feature point at (x+Δx, y+Δy) in frame *i+1*.

For making computation simpler and quicker the real world three dimensional (3-D+time) objects are transferred to a (2-D+time) case. Then the thoracic image can be described by the 2-D dynamic brightness function of $I(x, y, t)$. Provided that in the neighborhood of the feature point, change of brightness intensity does not happen in the motion field, following expression can be used:

$$I(x, y, t) = I(x + \delta x, y + \delta y, t + \delta t) \tag{3}$$

Taylor series is used for the right-hand side of the above equation, to obtain:

$$I(x + \delta x, y + \delta y, t + \delta t) = I(x, y, t) + \frac{\partial I}{\partial x}\Delta x + \frac{\partial I}{\partial y}\Delta y + \frac{\partial I}{\partial t}\Delta t + \text{Higher order terms (H.O.T.)} \tag{4}$$

From equations 3 and 4; neglecting the higher order terms,

$$\frac{\partial I}{\partial x}\Delta x + \frac{\partial I}{\partial y}\Delta y + \frac{\partial I}{\partial t}\Delta t = 0 \tag{5}$$

Dividing the terms in equation 5 by Δt on both sides (to get the equation in terms of x, y component velocity)

$$\frac{\partial I}{\partial x}\,{}^{\Delta x}\!/_{\Delta t} + \frac{\partial I}{\partial y}\,{}^{\Delta y}\!/_{\Delta t} + \frac{\partial I}{\partial t} = 0 \tag{6}$$

where ${}^{\Delta x}\!/_{\Delta t} = V_x$, ${}^{\Delta y}\!/_{\Delta t} = V_y$; thus,

$$\frac{\partial I}{\partial x}V_x + \frac{\partial I}{\partial y}V_y + \frac{\partial I}{\partial t} = 0 \tag{7}$$

Where V_x and V_y are the x and y components of velocity or optical flow of $I(x, y, t)$; $\frac{\partial I}{\partial x}$, $\frac{\partial I}{\partial y}$ and $\frac{\partial I}{\partial t}$ being the spatio-temporal derivatives of $I(x, y, t)$

$$I_x.v_x + I_y.v_y = -I_t \tag{8}$$

Vector representation being

$$\nabla I.\vec{v} == -I_t \tag{9}$$

Where ∇I is the spatial gradient of brightness intensity and $\vec{v}$ is the optical flow (velocity vector) of the previously detected feature points, I_t being the time derivative of the brightness intensity. This flow of a feature point (x, y) across a sequence of image frames is shown in figure 2.

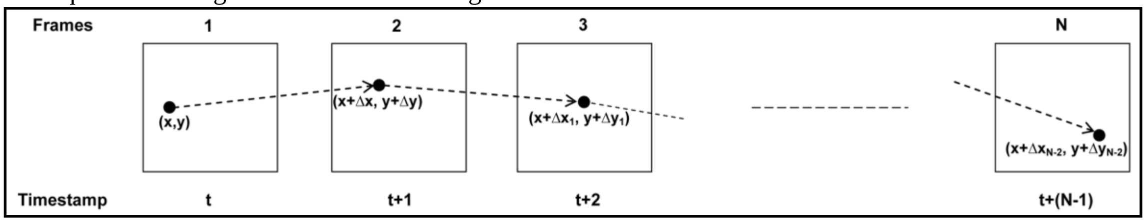

Figure 2: Flow of a common feature point (x, y) through a sequentially temporal thoracic image sequence with N frames, arrows indicating the changing velocity vector $\vec{v}$.

Result and Discussion:-

The feature detector/descriptor implemented on the temporal image sequence gave out matching feature points among the six continuous frames of the thoracic continuous temporal image sequence $(0.1 \le t \le 0.6)$ where t is the timestamp of frames in the sequence for all Anatomical Positions (AP) with average translation values as seen in tables 2 to 4 & figures 3 & 4 below.

Table 2: Average translation for all 10 subjects against inter-frame durations in Axial AP

AXIAL Average translation (pixels)										
slices	**case1**	**case2**	**case3**	**case4**	**case5**	**case6**	**case7**	**case8**	**case9**	**case10**
1	0.046561	0	0.049624	0.128273	0.102524	0.122075	0.104956	0.081344	0.147959	0.235239
2	0.073944	0.054379	0.211599	0.263143	0.220326	0.191888	0.172506	0.176225	0.156951	0.234938
3	0.121425	0.089757	0.07818	0.260438	0.217009	0.23198	0.16049	0.196808	0.154188	0.491434
4	0.23625	0.040567	0.077135	0.120165	0.335052	0.223568	0.123352	0.236095	0.272783	0.549633
5	0.164686	0.087393	0.235022	0.054348	0.229467	0.276633	0.174664	0.226786	0.346062	0.414524

Table 3: Average translation for all 10 subjects against inter-frame durations in Coronal AP

CORONAL Average translation (pixels)										
slices	**case1**	**case2**	**case3**	**case4**	**case5**	**case6**	**case7**	**case8**	**case9**	**case10**
1	0.048984	0.241160	0.090254	0.337341	0.089902	0.272166	0.413222	0.316280	0.705058	0.388508
2	0.256533	0.444705	0.283750	0.441339	0.545150	0.444112	0.574094	0.563048	1.515027	0.586950
3	0.544413	0.451036	0.490317	0.435855	0.574323	0.433924	0.547459	0.600381	1.540612	2.593868
4	0.554775	0.395562	0.443058	0.414418	0.617033	0.458451	0.522414	0.699724	1.507699	0.706559
5	0.360829	0.380994	0.528879	0.494821	0.682199	0.532425	0.503148	0.645080	1.431860	0.585679

Table 4: Average translation for all 10 subjects against inter-frame durations in Sagittal AP

SAGITTAL Average translation (pixels)										
slices	**case1**	**case2**	**case3**	**case4**	**case5**	**case6**	**case7**	**case8**	**case9**	**case10**
1	0.056349	0.101943	0.033191	0.197714	0.021831	0.218298	0.283102	0.387337	0.318476	0.347647
2	0.066874	0.037726	0.030762	0.224660	0.080744	0.514823	0.450867	0.602718	0.410166	0.438517
3	0.228785	0.144020	0.036248	0.183792	0.130526	0.511193	0.503673	0.639201	0.335686	0.476230
4	0.119935	0.124705	0.041039	0.228293	0.091893	0.482862	0.573929	0.666332	0.373603	0.521382
5	0.131468	0.042193	0.026666	0.237422	0.078702	0.544569	0.504332	0.658937	0.326333	0.505156

The feature points are color coded with respect to the indices and IDs assigned to them throughout the process. The trails they leave (see figure 3) after motion also exhibit the same color combination as assigned to respective feature points. The translations obtained are inherently in pixel units. With the knowledge of PPI (pixel per inch) value of the respective images in question, the displacements can be converted into more tangible units. A corresponding registered image representation is shown as figure 3.

Figure 3: (a) The color coded feature points and their colored trails showing the distinct paths for Sagittal AP 'case 5'; (b) The registered image for the corresponding sequence.

As we can see in figure 4 (a), the axial translations were recorded highest for subject 'case 10' and the lowest corresponding values for 'case 2'. The average value for 'case 10' was recorded at 0.3851 pixels, which was way above the population average of 0.184 shown by a line across the plot. In case of coronal AP as can be seen in figure 4 (b), the biggest deformations throughout the sequence are exhibited by the subjects 'case 10' and 'case 9' at 2.594 and 1.54 pixels respectively. The population average in this case being 0.5847 marked by a straight line in the corresponding plot. Though apart from 'case 10' only 'case 9'exhibited bigger deviations than the average value, the change in deformation with respect to inter-frame durations was more or less constant; on the other hand 'case 10' exhibited enormous shift from the average value while transitioning from 3rd frame to 4th frame. Looking at figure 4 (c) for the sagittal AP, all subjects though a bit above and below the average maintain an almost constant rate of change in the deformations and do not exactly exhibit any erratic patterns through the observed full inhale to exhale process.

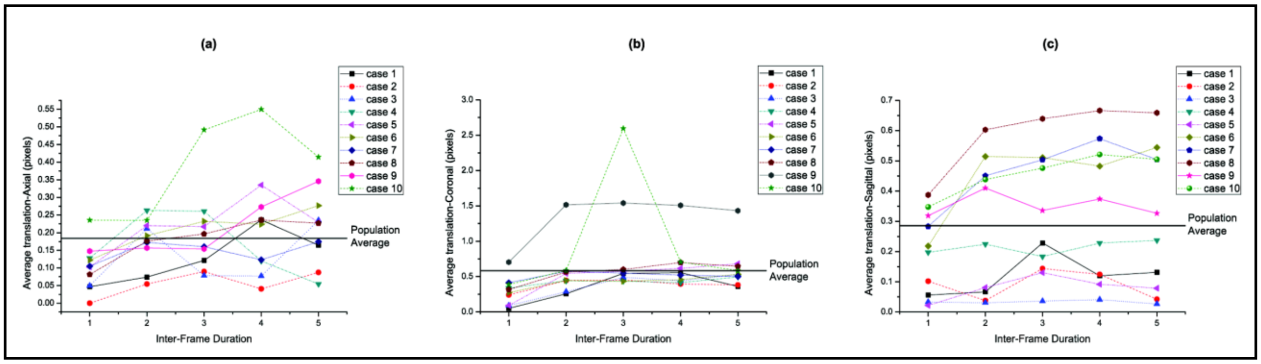

Figure 4: Average translations for all subjects in (a) axial, (b) coronal & (c) sagittal APs respectively

After having a comprehensive look at all subjects' deformation pattern data through axial, coronal and sagittal APs collectively, it was inferred that subject 'case 10' singled out as the only one with maximum deformation. This analysis indicates anomalous breathing patterns from the aforementioned subject among the considered consensus average.

Conclusion:-

A framework has been presented showing how to use a feature point set generated using a Hessian-matrix based feature detector and Haar wavelets based descriptor such as SURF through a motion estimation technique such as OFM tracking for deformable image transformations in medical images such as the thoracic 'pectus excavatum' [10, 12] full exhale and full inhale used in this work.

This conclusion is of high clinical relevance from a diagnostic point of view as well; the artifacts and position uncertainties due to uneven breathing patterns which hamper the image guided clinical interventions can be corrected to a point where there influence on the actual data and the diagnostics based on them is brought down to the least.

This work can be looked upon as an automatic way of deformable image registration for high contrast medical images using landmark (control) points. Although the proposed methodology provides with a fast and accurate way of DIR for medical images and thus an account of deformity in the thoracic periphery, there is much scope for improvement in the overall process. One way this can be achieved in future is by modifying the SURF and/or the Motion estimation procedure involved in the process. Another way is to improve and enhance the quality as well as the quantity of the database used. Also, the aforementioned procedure can provide better results if applied for a different human anatomy altogether.

However diligently and accurately it may have been done, there might still be some scope of improvement and betterment in the methodology and also in its presentation. The search and pursuit of better methods for deformable medical image registration is still on.

References:-

1. Aires KRT, Santana AM, Medeiros AAD (2008) Optical Flow Using Color Information (PDF). ACM New York, NY, USA. ISBN 978-1-59593-753-7.
2. Barron JL, Fleet DJ, Beauchemin S (1994) Performance of optical flow techniques. International Journal of Computer Vision (Springer).
3. Bay H, Ess A, Tuytelaars T, Van Gool L (2008) SURF: Speeded Up Robust Features. Computer Vision and Image Understanding (CVIU), Vol. 110, No. 3, pp. 346--359.
4. Bay H, Tuytelaars T, Van Gool L (2006) in Computer Vision – ECCV 2006, Edited by Aleš Leonardis , Horst Bischof and Axel Pinz, Springer Berlin Heidelberg, Zurich , Vol. 3951, pp 404-417.
5. Beauchemin SS, Barron JL (1995) The computation of optical flow. ACM-New York, USA.
6. Blackall JM, Ahmad S, Miquel ME, McClelland JR, Landau DB, Hawkes DJ (2006) MRI-based measurements of respiratory motion variability and assessment of imaging strategies for radiotherapy planning. Phys. Med. Biol., vol. 51, no. 17, pp. 4147–4169.
7. Cornelis N, Van Gool L (2008) Fast scale invariant feature detection and matching on programmable graphics hardware. Proceedings of IEEE Computer Society Conference on Computer Vision and Pattern Recognition Workshops, IEEE, pp1-8, June 23-28.

8. Ehrhardt J, Werner R, Schmidt-Richberg A, Handels H (2011) Statistical Modeling of 4D Respiratory Lung Motion Using Diffeomorphic Image Registration. IEEE Transactions on Medical Imaging. Doi:10.1109/TMI.2010.2076299.
9. Goitein M (2004) Organ and tumor motion: An overview. Seminars in Radiation Oncology, 14, 2–9.
10. Haller JA, Kramer SS, Lietman (1987) A Use of CT scans in selection of patients for pectus excavatum surgery: a preliminary report. Journal of pediatric surgery 22, 904-906.
11. Keall PJ, Mageras GS, Balter JM et al (2006) The management of respiratory motion in radiation oncology report of AAPM task group 76. Med. Phys., vol. 33, no. 10, pp. 3874–3900.
12. Kim H, Park H, Nam K et al (2010) Fully automatic initialization method for quantitative assessment of chest-wall deformity in funnel chest patients. Medical & Biological Engineering & Computing. Springer. Doi: 10.1007/s11517-010-0612-3.
13. Koenderink JJ (1984) The structure of images, Biological Cybernetics. Springer 50, 363-370.
14. Lindeberg T (1998) Feature detection with automatic scale selection. International journal of computer vision 30, 79–116.
15. Mikolajczyk K, Schmid C (2001) Indexing based on scale invariant interest points. Proceedings of Eighth International Conference on Computer Vision, IEEE.
16. Modersitzki J (2004) Numerical Methods for Image Registration. Oxford University Press.
17. Muenzing SEA, Van Ginnekan B, Viergever MA, Pluim JPW (2014) DIRBoost-an algorithm for boosting deformable image registration: application to lung CT intra-subject registration. Medical Image Analysis, Elsevier 18, 449-459.
18. Nehmeh SA, Erdi YE, Pan T et al (2004) Quantitation of respiratory motion during 4D-PET/CT acquisition. Med. Phys., vol. 31, no. 6, pp. 1333–1338, 2004.
19. Oliviera FPM, Tavares JMRS (2012) Medical Image Registration: a Review. Computer methods in Biomechanics and Biomedical Engineering 17, 73-93.
20. Peyrat JM, Delingette H, Sermesant M, Pennec X, Xu C, Ayache N (2008) Registration of 4D time-series of cardiac images with multichannel diffeomorphic demons. Proceedings of the Medical Image Computing and Computer-Assisted Intervention, Springer.
21. Reinhardt JM, Ding K, Cao K, Christensen GE, Hoffman EA, Bodas SV (2008) Registration-based estimates of local lung tissue expansion compared to Xenon CT measures of specific ventilation. Med. Image Anal., vol. 12, no. 6, pp. 752–763.
22. Sarrut D, Boldea V, Miguet S, Ginestet C (2006) Simulation of four-dimensional CT images from deformable registration between inhale and exhale breath-hold CT scans. Med. Phys., vol. 33, no. 3, pp. 605–617.
23. Sato AK, Stevo NA, Tavares RS, Tsuzuki MSG, Kadota E, Gotoh T, Kagei S, Iwasawa T (2011) Registration of temporal sequences of coronal and sagittal MR images through respiratory patterns. Biomedical Signal Processing and Control. Doi:10.1016/j.bspc.2010.08.002.
24. Sotiras A, Davatzikos C, Paragios N (2013) Deformable Medical Image Registration: A Survey. IEEE Transactions on Medical Imaging 32, 1153-1190.
25. Stevo N, Campos R, Tavares RS, Tsuzuki MDSG, Gotoh T, Kagei S, Iwasawa T (2009) Registration of temporal sequences of coronal and sagittal images obtained from magnetic resonance. Proceedings of XX International Congress of Mechanical Engineering.
26. Sun D, Roth S, Black MJ (2014) A Quantitative Analysis of Current Practices in Optical Flow Estimation and the Principles Behind Them. International Journal of Computer Vision, Springer US, Vol. 106, Issue 2, 115-137.
27. Thirion JP (1998) Image matching as a diffusion process: An analogy with Maxwell’s demons. Medical Image Analysis, Elsevier 2,243-260.
28. Thomson W (1874) Kinetic theory of the dissipation of energy. Nature 9, pp 441–444.
29. Tsui BMW, Segars WP, Lalush DS (2000) Effects of Upward Creep and Respiratory Motion in Myocardial SPECT. IEEE Transactions on Nuclear Science, v. 47, pp. 1192-1195.
30. Vedam SS, Keall PJ, Docef A, Todor DA, Kini VR, Mohan R (2004) Predicting respiratory motion for four-dimensional radio-therapy. Med. Phys., vol. 31, no. 8, pp. 2274–2283.
31. Viola P, Jones M (2001) Rapid object detection using a boosted cascade of simple features. Proceedings of the 2001 IEEE Computer Society Conference on Computer Vision and Pattern Recognition.
32. Warren DH, Strelow ER (1985) Electronic Spatial Sensing for the Blind: Contributions from Perception. Springer. ISBN 90-247-2689-1.

33. Yeo BTT, Sabuncu MR, Vercauteren T, Ayache N, Fischl B, Golland P (2010) Spherical demons: Fast diffeomorphic landmark-free surface registration. IEEE Transactions on Medical Imaging 29, 650-668.
34. Zordan VB, Celly B, Chiu B, DiLorenzo PC (2004) Breathe Easy: Model and Control of Simulated Respiration for Animation. Proceedings of the 2004 ACM SIGGRAPH/Eurographics symposium on Computer animation, Grenoble, France.